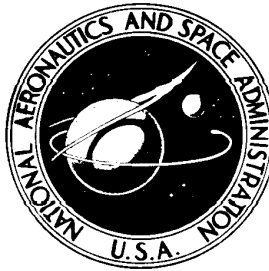**NASA TECHNICAL MEMORANDUM**

UB
NASA TM X-1809

OPERATIONAL EXPERIENCES AND CHARACTERISTICS OF THE M2-F2 LIFTING BODY FLIGHT CONTROL SYSTEM

by Weneth D. Painter and Berwin M. Kock

Flight Research Center
Edwards, Calif.

NATIONAL AERONAUTICS AND SPACE ADMINISTRATION • WASHINGTON, D. C. • JUNE 1969

OPERATIONAL EXPERIENCES AND CHARACTERISTICS OF THE

M2-F2 LIFTING BODY FLIGHT CONTROL SYSTEM

By Weneth D. Painter and Berwin M. Kock
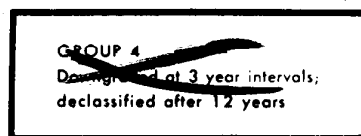
Flight Research Center
Edwards, Calif.

GROUP 4
Downgraded at 3 year intervals;
declassified after 12 years

NATIONAL AERONAUTICS AND SPACE ADMINISTRATION

OPERATIONAL EXPERIENCES AND CHARACTERISTICS OF THE

M2-F2 LIFTING BODY FLIGHT CONTROL SYSTEM*

By Weneth D. Painter and Berwin M. Kock
Flight Research Center

SUMMARY

Flights of the M2-F2 lifting body demonstrated that the manual control system and the stability augmentation system met the operational flight control requirements for the test vehicle. The regions of pilot-induced oscillation predicted from ground simulation were encountered in flight. The pilots considered the control system to be adequate for the M2-F2 flight envelope flown.

Limit-cycle data obtained during ground tests agreed with flight results. Structural frequencies of the vehicle control surfaces were never sustained in flight as a result of filtering in the stability augmentation system.

INTRODUCTION

With the increasing interest in space research, considerable effort is being devoted to developing a reentry vehicle that will combine some of the design and operational simplicity of a capsule with the mission flexibility of a piloted maneuverable reentry vehicle. Experience in landing low-lift-to-drag ratio airplanes indicated that a lifting-body vehicle could be landed. The hypothesis was proved with a lightweight lifting body, the M2-F1 (refs. 1 to 4). The M2-F2, which is a follow-on, heavyweight version of the M2-F1, was built under contract to NASA specifications and was delivered in June 1965 for flight testing at subsonic and low supersonic speeds. The general shape of the M2-F1 vehicle was retained, but a more sophisticated control system was designed to enable the pilot to improve the controllability and maneuverability of the vehicle. The design of the flight control system emphasized simplicity and reliability. Standard aircraft design practices were followed and existing off-the-shelf hardware was used where practical.

Flight tests with the M2-F2 were conducted by a joint U.S. Air Force and NASA Flight Research Center flight-test team at Edwards Air Force Base, Calif. On the sixteenth flight in May 1967, the vehicle was extensively damaged on landing.

This paper describes the M2-F2 flight control systems and discusses the design problems encountered during ground checkout, as well as the performance of the control

---

*Title, Unclassified.

system in flight. Other flight results from the program are presented in references 5 to 7.

SYMBOLS

The units used for the physical quantities defined in this section are given both in U.S. Customary Units and in the International System of Units (SI) (see ref. 8).

A	control-surface area, feet^2 (meters^2)
b	body reference span, feet (meters)
C_h	hinge-moment coefficient
C_{h_l}	lower-flap hinge-moment coefficient
C_{h_r}	rudder hinge-moment coefficient
C_{h_u}	upper-flap hinge-moment coefficient
c	body reference longitudinal length, feet (meters)
$\bar{c}$	distance from hinge line to centroid of control surface, feet (meters)
g	acceleration due to gravity, feet/second^2 (meters/second^2)
h	pressure altitude, feet (meters)
I_X	moment of inertia of the vehicle about the X-axis, slug-foot^2 (kilogram-meter^2)
I_{XZ}	product of inertia of the vehicle
I_Y	moment of inertia of the vehicle about the Y-axis, slug-foot^2 (kilogram-meter^2)
I_Z	moment of inertia of the vehicle about the Z-axis, slug-foot^2 (kilogram-meter^2)
$(K_{flight})_{max}$	maximum SAS gain at which the vehicle could be flown, degree/degree/second
K_I	rudder-to-aileron interconnect ratio, $-\dfrac{\delta_r}{\delta_a}$

2

K_p roll-damper gain, $\dfrac{\delta_a}{p}$, degree/degree/second

K_q pitch-damper gain, $\dfrac{\delta_l}{q}$, degree/degree/second

K_r yaw-damper gain, $\dfrac{\delta_r}{r}$, degree/degree/second

K_{sr} **gain at which structural resonance occurs, degree/degree/second**

$\left(L_{\delta_a}\right)_{eff}$ **roll-control power,** $\dfrac{\text{Moment per} \left(\delta_a + K_I \delta_a\right)}{I_X}$, **radians/second^2/radian**

M **Mach number**

M_{δ_l} **pitch-control power,** $\dfrac{\text{Moment per } \delta_l}{I_Y}$, **radians/second^2/radian**

N_{δ_r} **yaw-control power,** $\dfrac{\text{Moment per } \delta_r}{I_Z}$, **radians/second^2/radian**

p **rolling velocity, degrees/second**

q **pitching velocity, degrees/second**

$\bar{q}$ **dynamic pressure, pounds/foot^2 (kilograms/meter^2)**

r **yawing velocity, degrees/second**

S **body planform reference area, feet^2 (meters^2)**

s **Laplace variable**

t **time, seconds**

W **weight, pounds (kilograms)**

α **angle of attack, degrees**

β **angle of sideslip, degrees**

Δp **limit-cycle roll-rate amplitude, peak to peak, degrees/second**

Δq **limit-cycle pitch-rate amplitude, peak to peak, degrees/second**

Δr **limit-cycle yaw-rate amplitude, peak to peak, degrees/second**

δ **control-surface deflection, degrees**

δ_a lateral-control deflection, $\delta_{u_L} - \delta_{u_R}$, degrees

δ_l lower-flap deflection, positive trailing edge down, degrees

δ_r rudder deflection, $\left(\delta_{r_R}\right)_{measured} + \left(\delta_{r_L}\right)_{measured}$, positive
        trailing edge left, degrees

$\delta_{r_{measured}}$ single rudder-surface deflection, degrees

δ_u upper-flap trim deflection, $\dfrac{\delta_{u_L} + \delta_{u_R}}{2}$, negative trailing edge up,
        degrees

φ bank angle, degrees

Subscripts:

L   left

R   right

DESCRIPTION OF THE VEHICLE AND FLIGHT CONTROL SYSTEMS

The M2-F2 (fig. 1), a single-place research lifting-body vehicle, is basically a
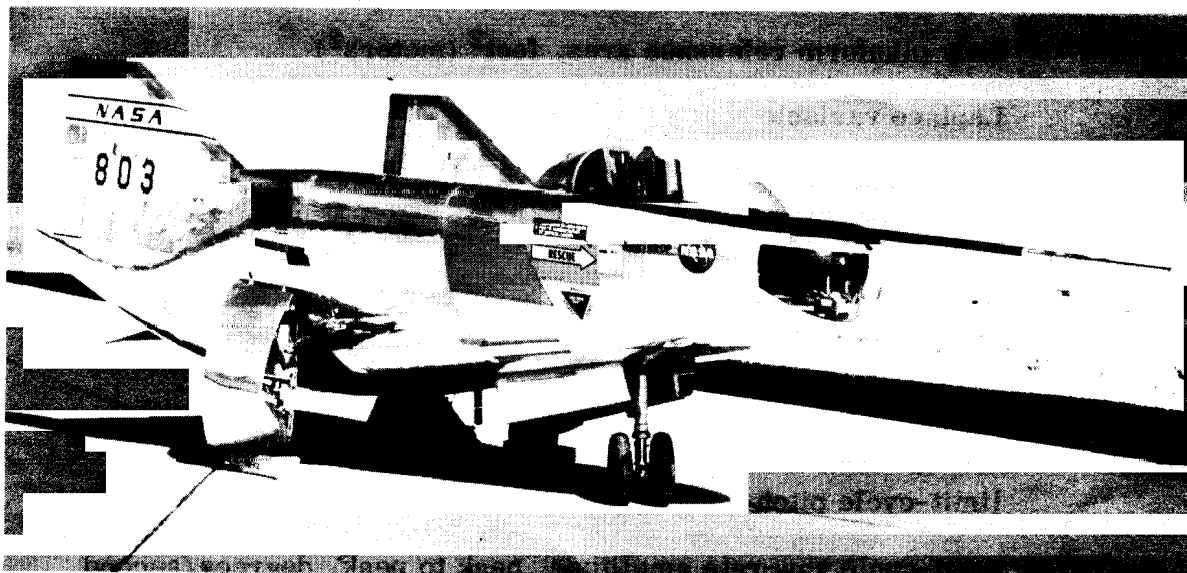boattailed 13° half cone with vertical end-plate-type fins near the rear of the vehicle.

Figure 1.— M2-F2 research vehicle.   *E-14332*

4

The vehicle is 22.2 feet (6.76 meters) long, 9.63 feet (2.94 meters) wide, and weighed approximately 6000 pounds (2722 kilograms) during the glide-flight program. It has a conventional tricycle landing gear which was extended in flight just prior to touchdown but could not be retracted in flight. Additional physical characteristics of the vehicle are presented in table I.

Five control surfaces are provided for aerodynamic control of the vehicle. A lower flap provides pitch control in response to longitudinal control-stick input and increased pitch damping by the stability augmentation system (SAS). The two upper flaps move in unison to provide pitch trim control and differentially for roll control and augmented roll damping by the SAS. The authorities of these surfaces are shown in figure 2. Control in yaw and increased yaw damping through the SAS are provided by displacement of the two rudder surfaces on the side fins.
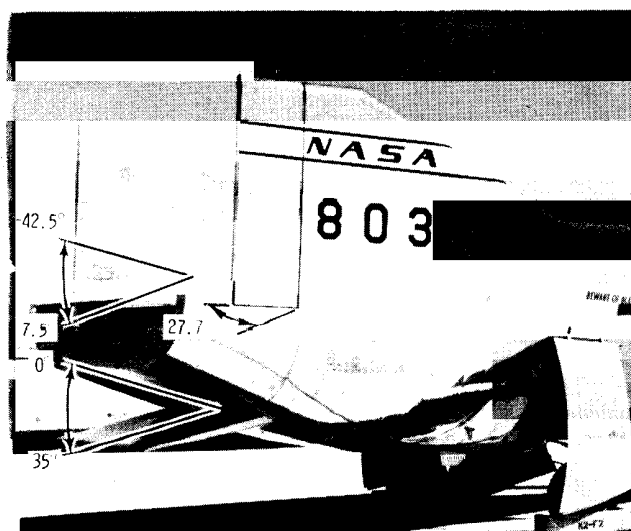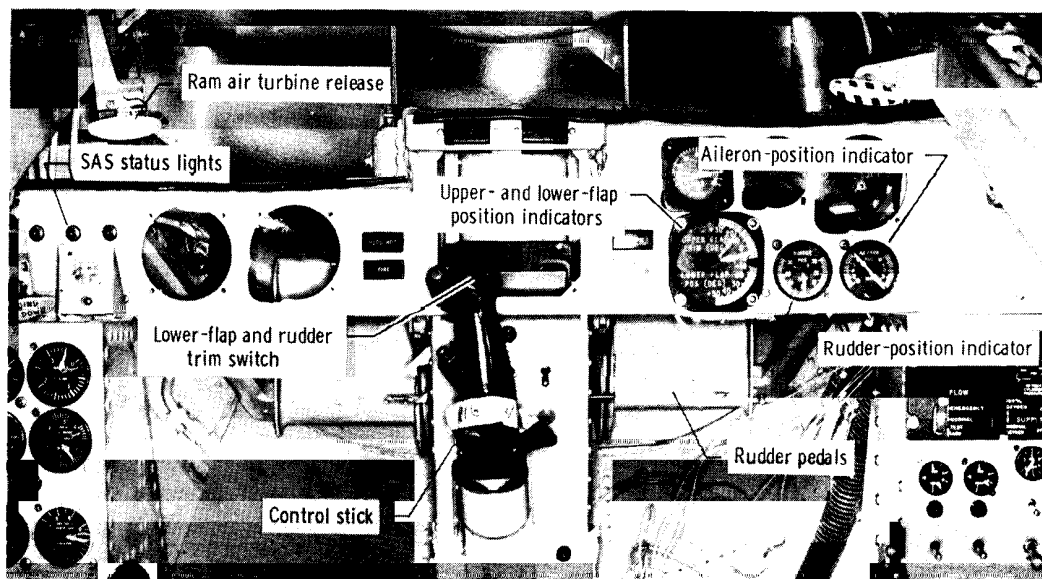

E-14334

Surface travel shown is maximum

Surface	Input	Travel, deg	Rate, deg/sec (1)
Lower flap	Trim	10 to 30	3
	Pitch stick	5 to 30	25
	Pitch SAS	±5	25
Upper flap	Pitch trim	0 to -35	15
	Aileron stick	±10	30
	Roll SAS	±5	30
Rudder	Trim	±5	20
	Pedal	±11	22
	Interconnect	±12.5	22
	Yaw SAS	±4.2	22

[1]Rates at 80 percent design hinge moment.
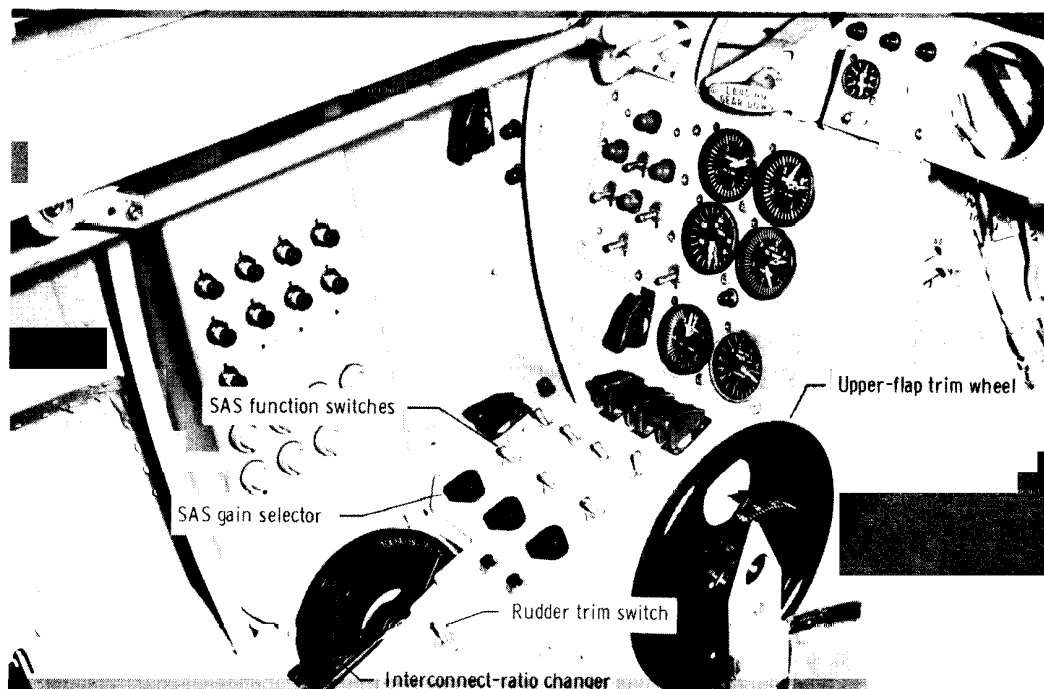
Figure 2.— M2-F2 control-surface authorities.

A conventional fighter-type cockpit (figs. 3(a) and 3(b)) was provided with a standard control stick and rudder pedals.

(a) Forward view.

E-13407

(b) Left-hand console.

E-13409

Figure 3.— M2-F2 cockpit arrangement.

PRIMARY FLIGHT CONTROL SYSTEM

General Description

The flight control system of the M2-F2 lifting body is an irreversible electro-mechanical hydraulic system with artificial feel for pitch, roll, and yaw control (figs. 4 and 5). The irreversible characteristics of the hydraulic system hold the control

Figure 4.– Schematic of M2-F2 longitudinal flight control system.

Figure 5.– Schematic of M2-F2 lateral-directional flight control system.

surface against any force that does not originate from the pilot's control movement and prevents these forces from being transmitted back to the pilot's controls. Pitch trim is accomplished by (1) changing the neutral (no-load) position of the artificial-feel system applied to the center stick and (2) repositioning the upper flaps. The lower flap provides pitch control. The upper flaps provide pitch trim and roll control. The rudders provide yaw control. A rudder-to-aileron interconnect is also provided to counteract the adverse yaw due to aileron deflection (discussed later). Augmentation of the aerodynamic damping in pitch, roll, and yaw is provided by a stability augmentation system, utilizing the aforementioned control surfaces.

The control stick is mechanically connected (by control cables and pushrods) to the hydraulic control valves on the actuators located at the upper flaps and the lower flap. Movement of the stick positions the control valves so that power from the hydraulic system is directed to the control-surface actuators to move the control surfaces. A mechanical follow-up system automatically closes off the flow of hydraulic fluid to the actuators when the desired control-surface deflection is reached.

Figure 6 shows that full-aft travel of the stick causes the lower flap to deflect to a position of 5° with reference to the bottom contour of the vehicle, and full-forward stick
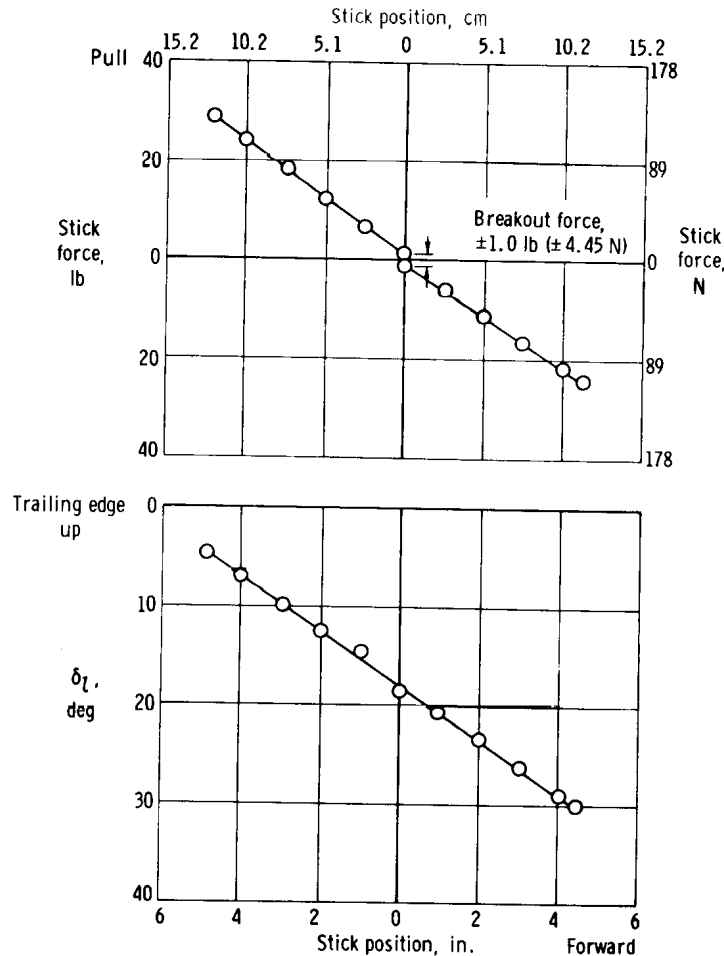

Figure 6.— M2-F2 longitudinal stick force and surface displacement as a function of stick position. Stick force and position measured at the pilot's grip (19.55-in. radius (49.6-cm radius)).

8

position causes the surface to position at 30°. The control-surface-to-stick gearing is 2.8 degrees/inch (1.10 degrees/centimeter), and the control-stick force gradient is 5.5 pounds per inch (9.7 newtons per centimeter) of stick travel.

Lateral travel of the control stick at the pilot's grip position is ±2.8 inches (±7.1 centimeters) which causes 10° of aileron deflection or ±5° surface differential from the upper-flap trim position, as shown in figure 7. The control-surface-to-stick gearing is 3.6 degrees per inch (1.4 degrees per centimeter) of stick travel. The control-stick force gradient is 3.1 pounds per inch (5.5 newtons per centimeter) of stick travel with a breakout force of 1.8 pounds (7.8 newtons).
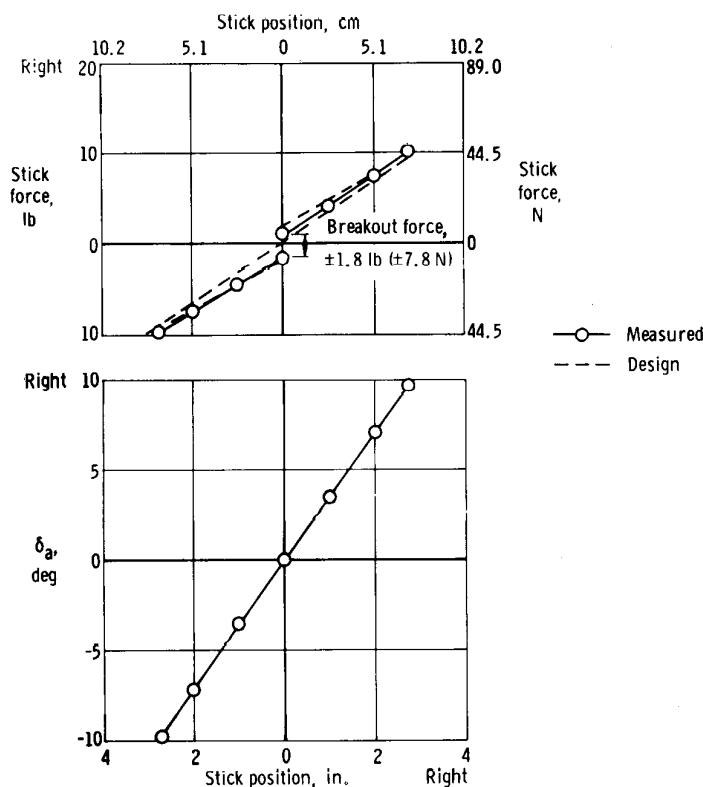

Figure 7.— M2-F2 lateral stick force and surface displacement as a function
of stick position. Stick force and position measured at the pilot's grip
(13.92-in. radius (35.35-cm radius)).

Primary controls for the rudders are conventional rudder pedals, mechanically connected to a hydraulic control valve at each rudder hydraulic actuator. The effective surface-to-pedal gearing for the two rudders is 4.0 degrees per inch (1.58 degrees per centimeter) for the deflection range of ±10°, as shown in figure 8. The surfaces operate about a 5° flared condition for the investigation reported herein, as illustrated in figure 8. In response to a pedal input, one surface moves out (increased deflection) as the other moves in (decreased deflection), although the rudders cannot move inboard farther than the faired or 0° deflection point. Figure 8 shows the pilot's pedal

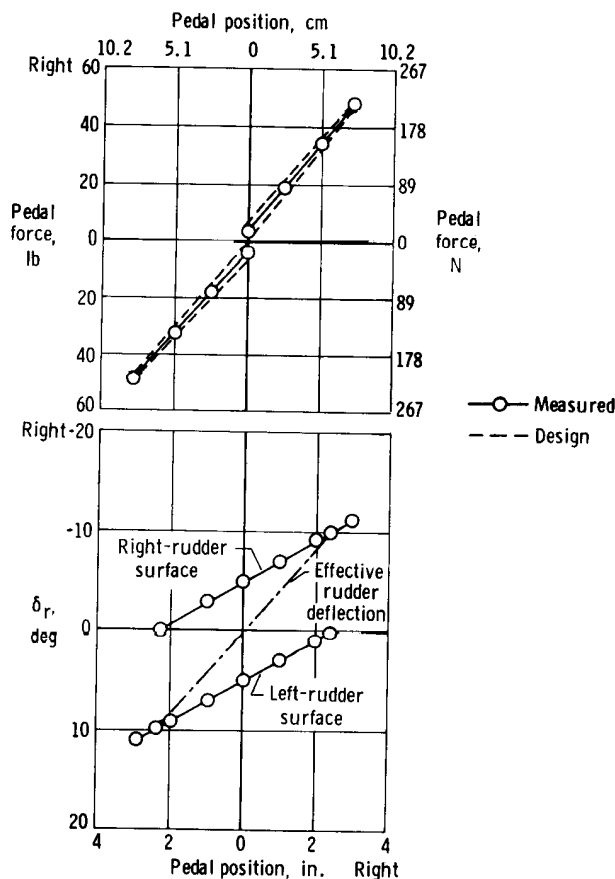force gradient, which is 16 pounds per inch (28.0 newtons per centimeter) of pedal deflection.

Figure 8.— M2-F2 pedal force and rudder displacement as a function of pedal position.

Artificial-Feel and Trim Systems

The artificial-feel system gives the pilot a sense of control feel under all flight conditions. Stick and rudder-pedal forces are provided by coil-spring bungees in the control system. The bungees apply loads to the pilot controls in proportion to stick or pedal movement, but the resultant feel has no relation to actual air loads. Pitch force trim is obtained by shifting the neutral "no-load" position of the feel bungee to a stick position corresponding to the desired lower-flap-surface position. Rudder trim is obtained by shifting the neutral "no-load" position of the feel bungee to a pedal position corresponding to the desired rudder-surface position. No aileron force trim is available from the cockpit, but it can be adjusted on the ground.
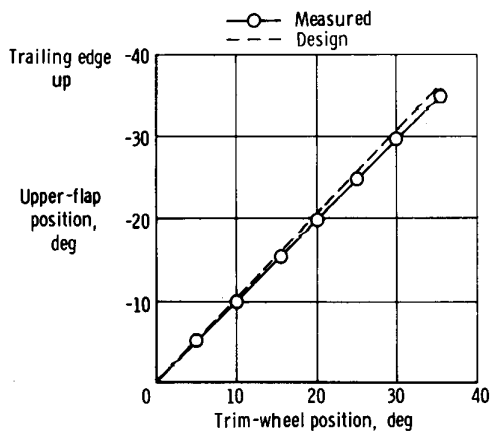
10

Figure 9.– M2-F2 pitch trim authority of upper flaps.

The upper-flap trim wheel controls the position of the upper flaps from 0° to -35°, as shown in figure 9.

Rudder-to-Aileron Interconnect System

The M2-F2 has a large dihedral effect. This dihedral effect combined with the yaw-due-to-aileron deflection results in a roll reversal throughout much of the flight region. To alleviate this problem an interconnect between the aileron and the rudder is necessary. The interconnect is a mechanical device to move the rudders with a movement of the ailerons. The interconnect is actuated by both pilot control and the stability augmentation system. The interconnect-ratio control wheel controls the amount of rudder deflection with respect to a given aileron deflection. The ratio of interconnect varies from 0 to 1.25. Figure 10 shows the variation of rudder deflection with aileron deflection for three specific values of interconnect ratio K_I.
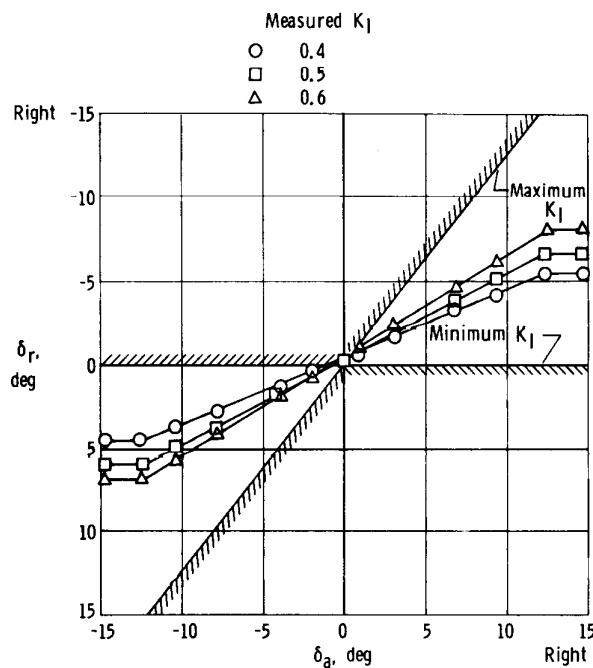

Figure 10.– Variation of M2-F2 rudder deflection with aileron deflection at various interconnect ratios.

The interconnect ratio has an important effect on the lateral-directional handling qualities. If too high an interconnect ratio is used, a pilot-airplane instability occurs. This problem becomes more severe at lower angles of attack and is also a function of

Mach number (refs. 6 and 7). Figure 11 illustrates that, at an angle of attack of 0° and a Mach number of 0.4, an instability occurs if the interconnect ratio is 0.5 or higher and a roll reversal occurs if the interconnect ratio is 0.3 or lower. At a Mach number of 0.9, however, an instability occurs at an interconnect ratio of 0.65 or higher, and a roll reversal would not occur even at an interconnect ratio of 0.
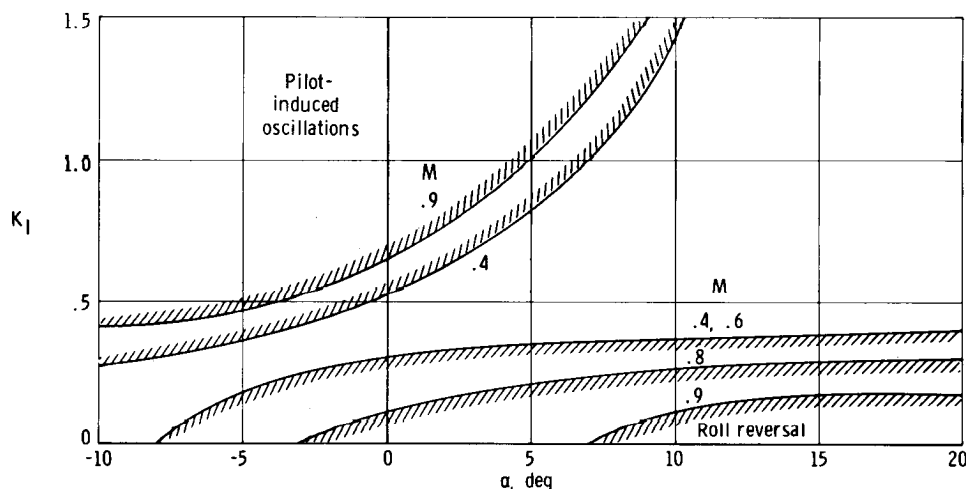

Figure 11.— Effect of interconnect ratio on lateral-directional controllability characteristics of the M2-F2, based on simulator studies.

Stability Augmentation System

The stability augmentation system provides damping inputs to the aerodynamic flight control system about the pitch, roll, and yaw axes. The SAS has three primary axes (pitch, roll, and yaw), each consisting of a functional or working channel and a monitor channel, and a single backup channel in pitch. The block diagram for the three axes is shown in figure 12. The functional channel in each axis is basically identical to the SAS from the F-5 and T-38 airplanes and consists of a rate gyro, an electronics assembly, protective circuit, and a hydraulic actuator. A monitor channel was added in each axis to detect malfunctions in the functional channel and to provide a fail-operate capability in pitch and fail-safe capability in roll and yaw. This is accomplished by comparing the feedback signal from the actuator with the signal from a model of the actuator in the monitor channel. If the difference between the feedback signal and the model signal exceeds a certain (adjustable) threshold, the comparator recognizes an error and switches either to pitch backup or to off for roll and yaw. For the flight investigation reported in this paper, the monitors were deactivated in roll and yaw.

The roll and yaw axes incorporated washout of steady rates. Washout was used to improve the vehicle handling qualities during turn maneuvers. Without washout the vehicle tends to be very sluggish.

The system is designed so that no single failure can disable all three axes. Similarly, no single failure can disable both the functional and backup pitch channels.

12

Internally, the power-distribution circuitry is so designed that the pitch and roll functional channels are separated from the pitch backup channel and yaw functional channel.
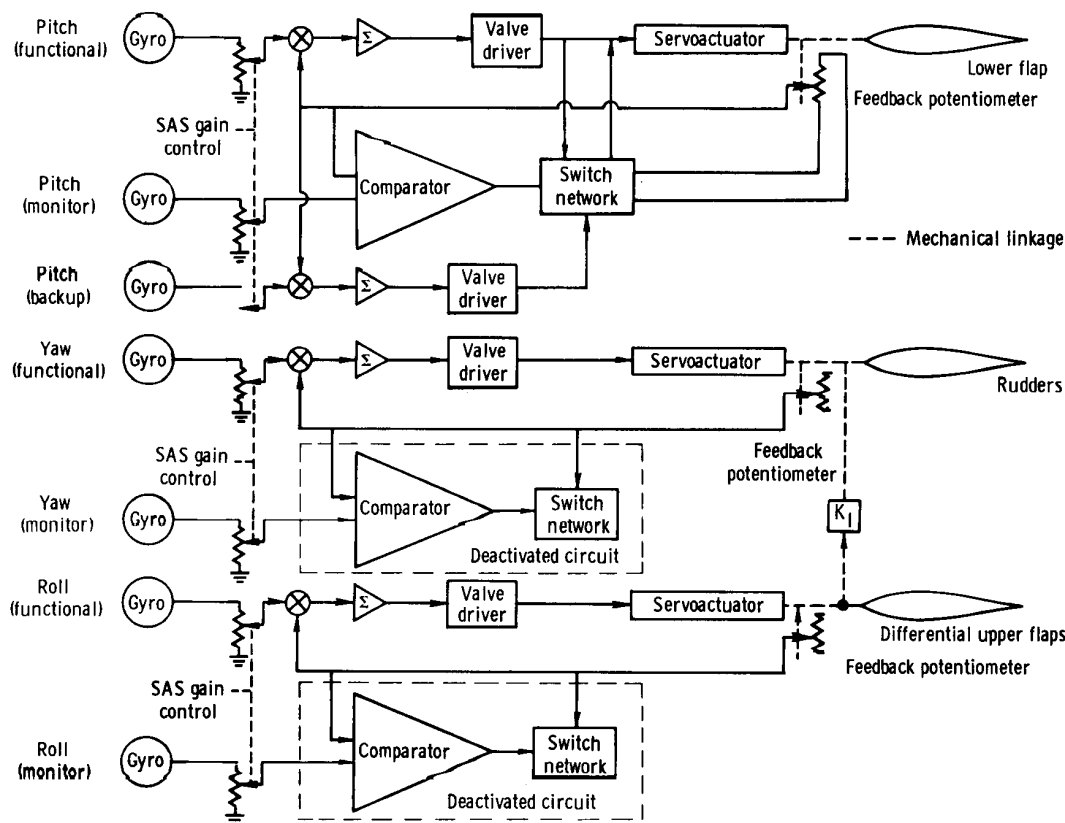

Figure 12.— Functional block diagram of M2-F2 stability augmentation system.

The controls for the SAS are in the cockpit on the left-hand pilot's console. The on-off switches are magnetically held when in the on position, and protective circuits around the servoactuator drive circuit cause the switch to disengage if a malfunction occurs. These protective circuits sense voltage levels.

Should a malfunction occur in the pitch functional channel, the system automatically switches to the pitch backup channel, and a warning light on the pilot's instrument panel is lit. A reset toggle switch permits the pilot to return to the functional pitch channel if a malfunction does not exist. Pitch backup can be selected manually by the pilot or automatically by the monitor in case of a malfunction.

The SAS gain selector in each axis controls the ratio of surface displacement to the angular rate signal through a variable resistor. The selector has 11 positions, 0 to 10, and system gain increases linearly to a maximum of 1 degree per degree per second at position 10 in all three axes.

Hydraulic Power Supply Systems

The vehicle has two 3000-psi hydraulic systems (fig. 13). The two systems have independent electric power and hydraulic pumps but operate simultaneously to supply vehicle hydraulic pressure. With both hydraulic systems operating, the control system has full hinge moment and maximum rate capability. When one hydraulic system fails, the system has only one-half the hinge-moment capability with the same maximum surface rate. The number one hydraulic system serves as the sole power source for the pitch and roll SAS servoactuators, with a ram air turbine backup hydraulic pump. The number two hydraulic system provides the sole hydraulic power source for the yaw SAS servoactuator.
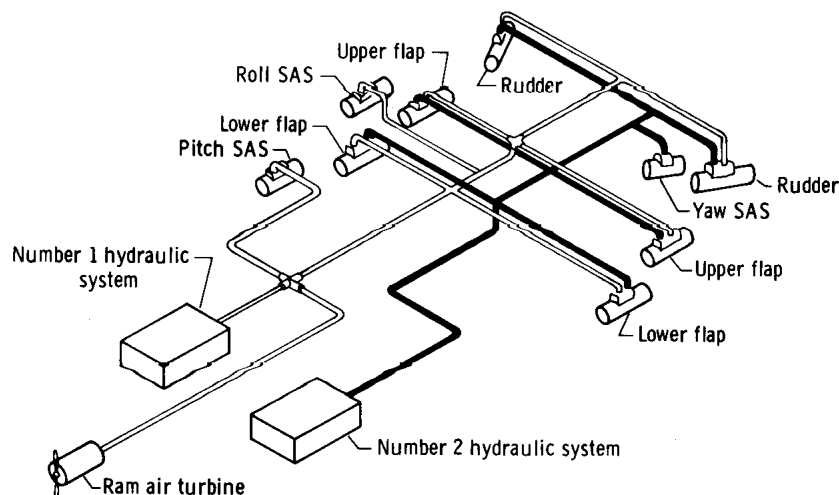

Figure 13.— Schematic of M2-F2 hydraulic systems. (Return lines not shown.)

CONTROL-SURFACE HINGE-MOMENT STUDIES

M2-F2 control-surface hinge-moment studies were made after the range of control-surface deflections required for flight was defined from wind-tunnel-model tests. Results of some of these hinge-moment studies are shown in figures 14(a) to 14(c). The approach used was to determine maximum hinge moments at all possible flight conditions within the flight boundaries for the vehicle.

The dimensions of the control surfaces are shown in table I; the following equation was used to compute the hinge moments:

$$\text{Hinge moment} = \bar{q}A\bar{c}C_h$$

The flight control system was designed by using the preceding equation with wind-tunnel hinge-moment coefficients as shown in figures 14(a) to 14(c).

(a) Upper flap hinge-moment data. $\delta_l = 45^o$.   (b) Lower-flap hinge-moment data. $\delta_u = -10^o$.   (c) Rudder hinge-moment data. $\delta_u = -10^o$; $\delta_l = 20^o$.
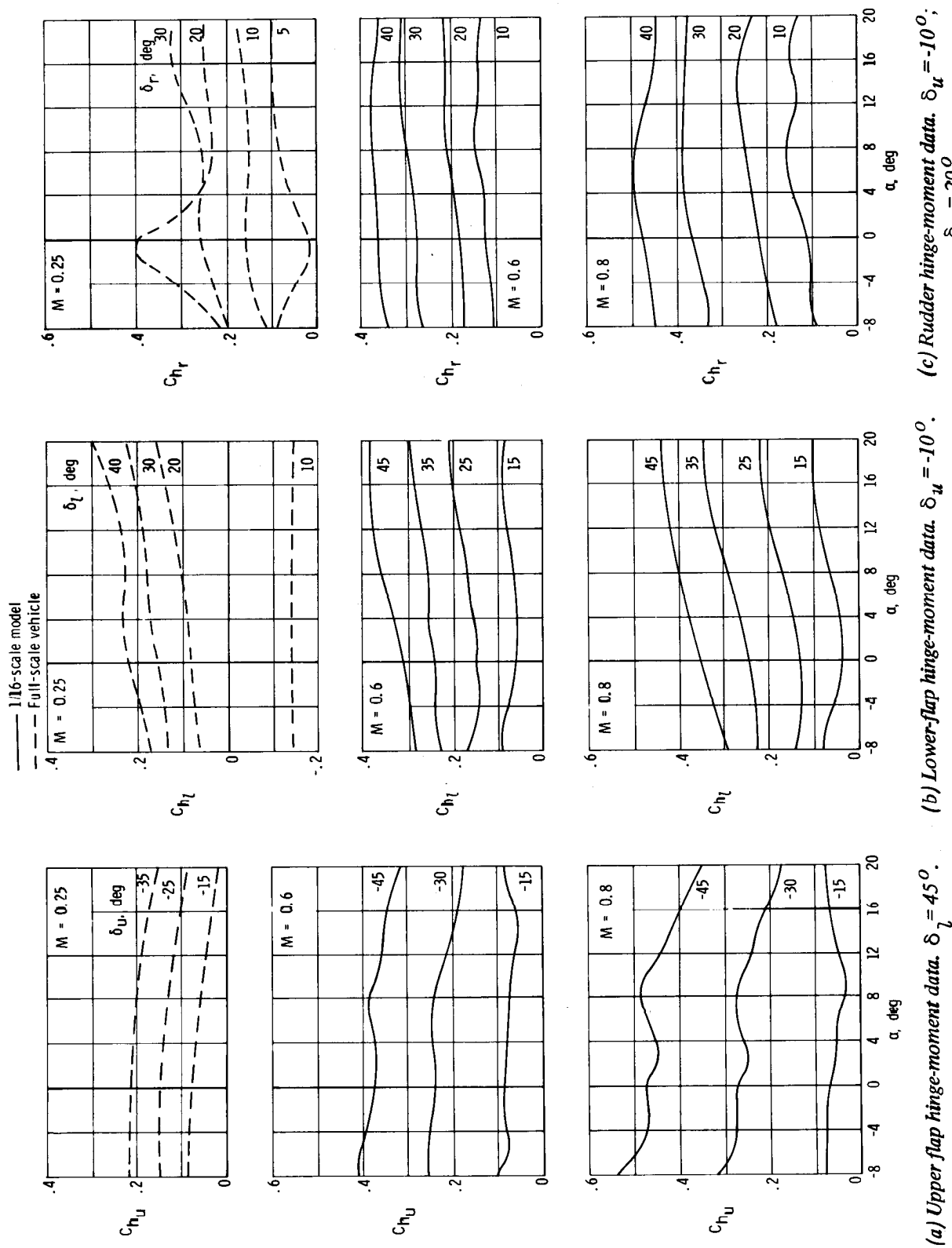
Figure 14.– Variation of M2-F2 control-surface hinge-moment coefficients with angle of attack obtained in wind tunnels for various control deflections. Data used for control-system design.

During the study, it was found that maximum hinge moments for each of the surfaces occurred at different flight conditions. For example, the maximum hinge moment of a fixed upper flap occurred at 0g or negative g at the lower angles of attack and high dynamic pressure with the lower flap at large deflections; whereas, the maximum hinge moment of a fixed lower flap occurred at high positive g and high angles of attack with the upper flap at large deflections.

SYSTEM-DEVELOPMENT PROBLEMS

During control-system checkout before the first flight, many problems were determined and system changes were required. The more important problems were SAS monitor channel tracking, SAS tripouts, structural resonance, limit cycles, and interconnect-ratio-linkage deadbands.

SAS Monitor Channel Tracking

As previously described, the SAS monitor channel was designed to disengage the functional channel if a difference in voltage occurred at the comparator input. Under normal operation, the model servo signal in the monitor channel was required to match the functional channel feedback signal in both magnitude and phase. In the roll and yaw axes, when washout was incorporated, this monitor channel tracking could not be accomplished, and the result was an unwanted tripout of a properly functioning channel.

It was discovered also that the fail-soft circuitry could cause a condition it was designed to prevent. The electronic switch that is operated by the comparator has sufficient leakage into the feedback path to cause a hard-over condition, yet offers enough impedance to prevent shutoff of the magnetic switch.

Since it was not possible to remedy the monitor-channel tracking condition without extensive redesign, it was decided to deactivate the monitor channel in the roll and yaw axes and reduce the SAS authority in the roll and yaw axes to a point where a hard-over condition would not be catastrophic.

SAS Nuisance Disengagements

During the operational ground tests on the SAS with all vehicle systems operating, it was found that electrical switching transients caused trip-outs in the functional pitch channel and transfers to the pitch backup channel. Transient voltage spikes were caused by various switches making the breaking contact. Diodes were installed across the switches to suppress the voltage spikes.

Inverter switching also caused loss of all SAS channels because of the electrical interruptions caused by switching from the SAS primary inverter to the SAS backup inverter. A 100-millisecond time-delay circuit was installed in the magnetic switch circuit of each SAS channel to keep the SAS from disengaging during the inverter switching.

16

Structural Resonance

During initial tests of the SAS, a structural-mode vibration was encountered. The structural vibrations were excited by placing the SAS gains at a high level and shaking the vehicle by hand. Vibrations from the control-surface motion were sensed by the gyros which transmitted signals to the control surface through the SAS, causing the control-surface oscillation to sustain itself with no external input. An illustration of a sustained pitch and roll oscillation of constant amplitude is presented in figure 15. The lightweight construction of the gyro mounting framework resulted in a 30-cps vibration, which was outside the operational bandwidth of the flight control system but degraded the system's capability and could have produced a structural failure.
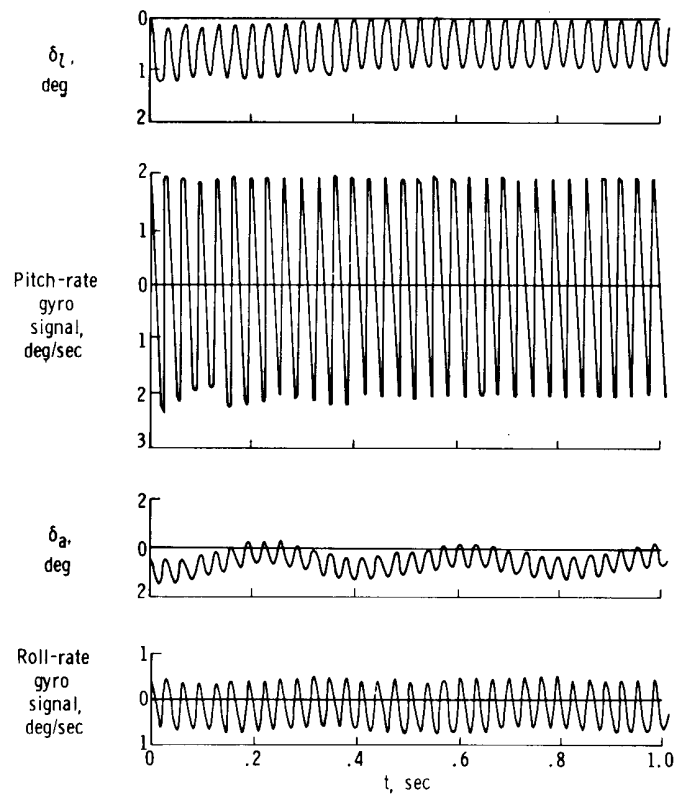
Figure 15.— M2-F2 sustained structural resonance during ground tests. Vehicle on wheels without structural-resonance filter in the SAS electronics; SAS gain position 5 for both pitch and roll.

The 30-cps resonance associated with the structure was a high enough frequency to be filtered without seriously deteriorating control response at lower frequencies. Stiffening the gyro platform assembly and installing a first-order-lag filter in the SAS electronics with a break frequency at 2 cps proved to be effective in eliminating any SAS response to the structural frequency, as shown in figures 16 and 17.
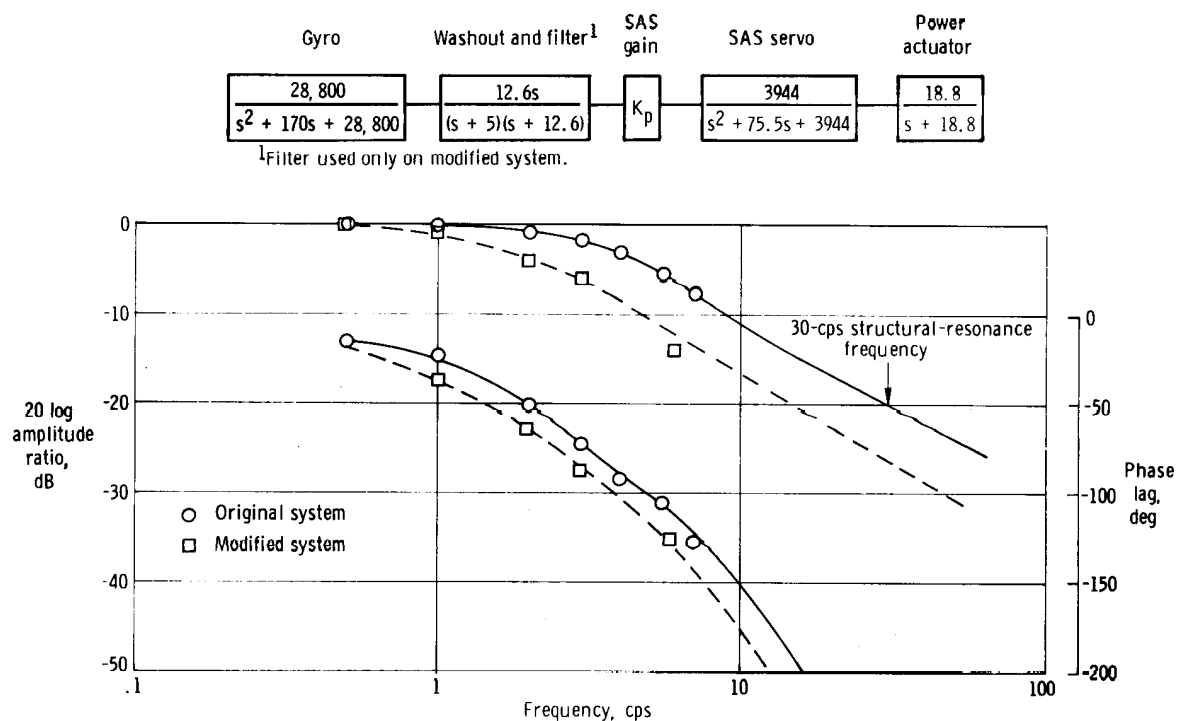
Gyro	Washout and filter[1]	SAS gain	SAS servo	Power actuator
$\dfrac{28,800}{s^2 + 170s + 28,800}$	$\dfrac{12.6s}{(s + 5)(s + 12.6)}$	K_p	$\dfrac{3944}{s^2 + 75.5s + 3944}$	$\dfrac{18.8}{s + 18.8}$

[1]Filter used only on modified system.

Figure 16.— Open-loop frequency response of the M2-F2 roll SAS from gyro to aileron surface.

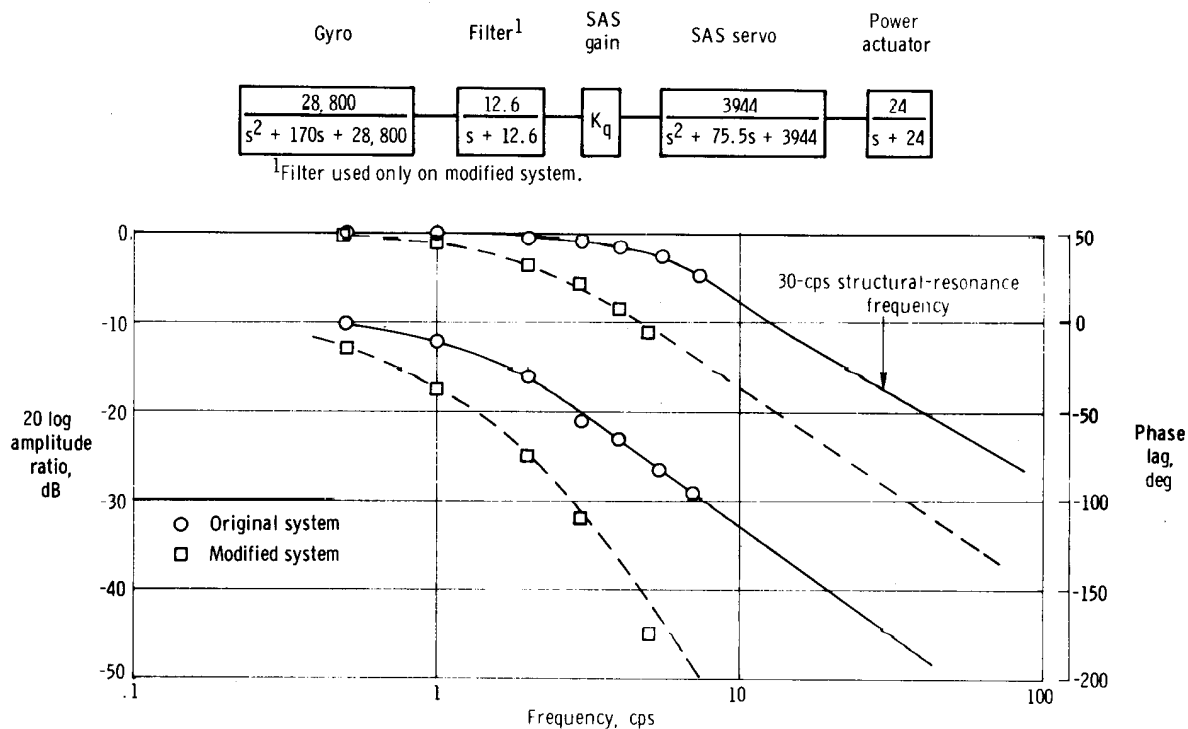| Gyro	Filter[1]	SAS gain	SAS servo	Power actuator
$\dfrac{28,800}{s^2 + 170s + 28,800}$	$\dfrac{12.6}{s + 12.6}$	K_q	$\dfrac{3944}{s^2 + 75.5s + 3944}$	$\dfrac{24}{s + 24}$

[1]Filter used only on modified system.

Figure 17.— Open-loop frequency response of the M2-F2 pitch SAS from gyro to lower-flap surface.

18

As shown in figure 16, the original system bandwidth was approximately 4 cps in roll (point at which open-loop response is -90° phase lag). The modified system, how-ever, has a bandwidth reduced by approximately 0.75 cps, brought about by the gain reduction (-6 dB) necessary to eliminate the response of the system to the 30-cps structural resonance.

The bandwidth of the original pitch system (fig. 17) was approximately 6.2 cps. The bandwidth of the modified system was reduced by 3.6 cps, which was again brought about by the gain reduction necessary to eliminate the response of the system to the 30-cps structural resonance.

Limit Cycle

Unacceptable limit cycles, or residual control-surface/vehicle oscillations caused by the stability augmentation system, were encountered during ground limit-cycle tests. Phase lag produced by control-system hysteresis, friction, and deadband caused the limit cycles, which existed in all three axes when the damper gain and control power were high (ref. 9).

Limit-cycle tests were made by using an analog computer to simulate the aero-dynamic loop around the stability augmentation system, as shown in figure 18. The
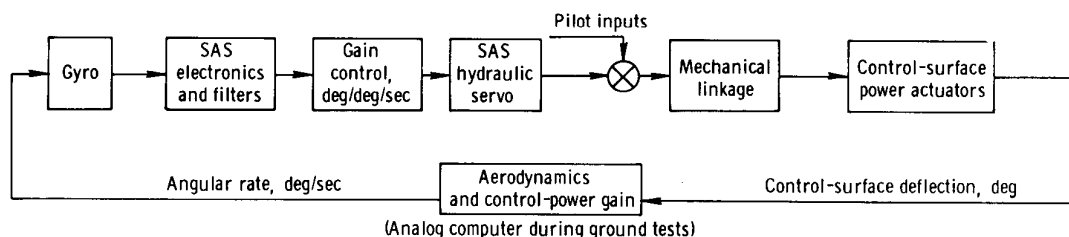

Figure 18.-- Block diagram of control system and external components used in M2-F2 SAS limit-cycle tests.

following simplified transfer functions relating rate to surface deflection were used:

$$\text{Pitch} \quad \frac{q(s)}{\delta_l(s)} = \frac{M_{\delta_l}}{s}$$

$$\text{Roll} \quad \frac{p(s)}{\delta_a(s)} = \frac{\left(L_{\delta_a}\right)_{eff}}{s}$$

$$\text{Yaw} \quad \frac{r(s)}{\delta_r(s)} = \frac{N_{\delta_r}}{s}$$

The s term in the denominator contributed a phase-angle lag of 90° between rate and

surface deflection. The simplification was conservative, since the aerodynamic lag would probably be less than 90°. The remaining 90° of phase lag necessary for a continuing limit-cycle oscillation came from the electronic filter, power actuator, and mechanical linkages.

The structural-resonance and limit-cycle problems involving the M2-F2 were analyzed by using the actual vehicle. It was necessary to consider the two problems simultaneously in the selection of a filter for the stability augmentation system.

The SAS gain ratio of structural-resonance gain to flight gain was established as

$$\frac{K_{sr}}{\left(K_{flight}\right)_{max}} = 2.0$$

Experience had shown that this criterion provided a reasonable safety margin against structural resonance in flight and, thus far, the criterion has proved to be satisfactory (ref. 9).

Figures 19 and 20 show the limit-cycle characteristics of the pitch and roll SAS axes, respectively. The curves in each figure illustrate the characteristics of the original system and the modified system. Flight experience at the Flight Research Center has shown that 0.5° peak-to-peak limit-cycle amplitude is the maximum allowable.
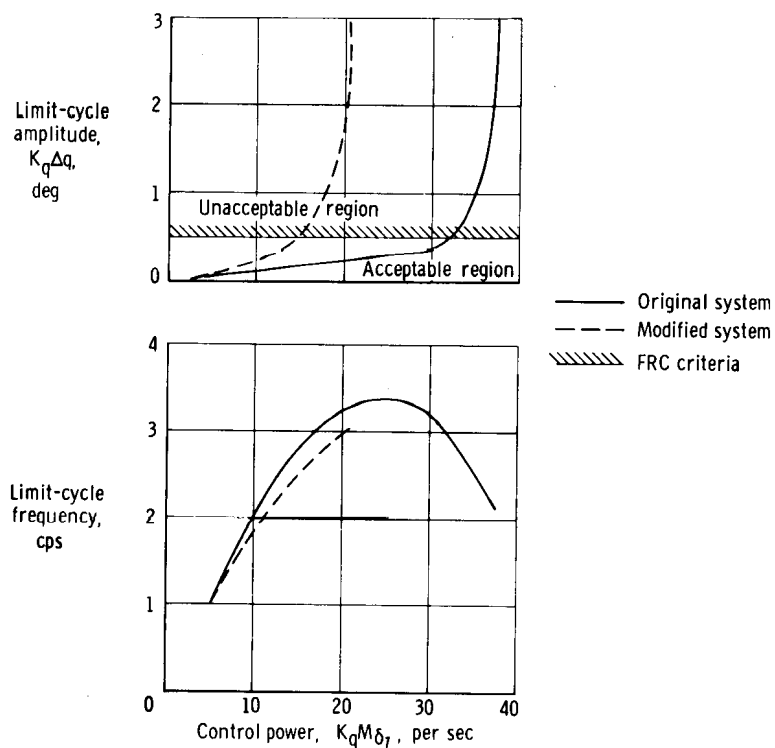

Figure 19.— M2-F2 limit-cycle characteristics of the pitch axis, based on ground tests.
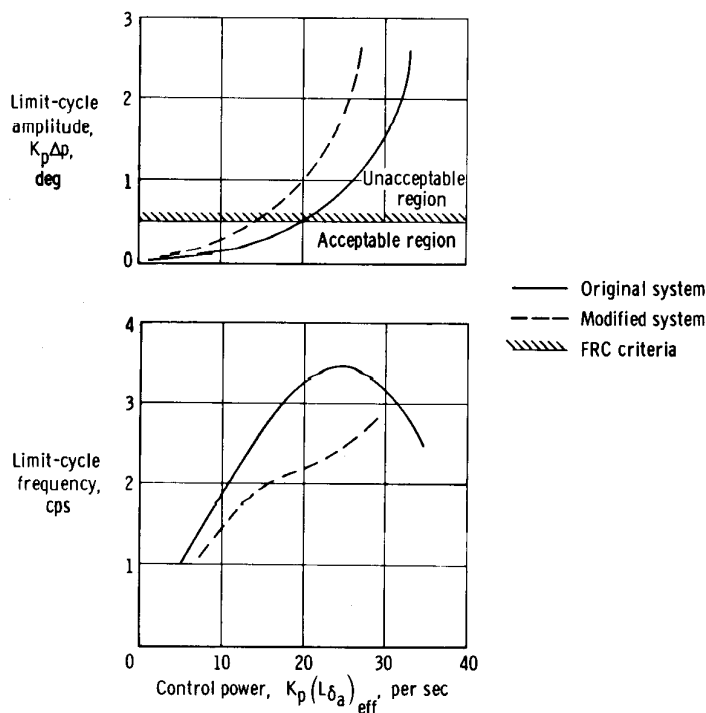
Figure 20.— M2-F2 limit-cycle characteristics of the roll axis, based on ground tests.

The filter (added to the SAS electronics) reduced the maximum usable control power, which is the penalty for suppressing the structural resonance. A notch filter at 30 cps would permit operation at higher SAS gain but has not been used because of the complex modification necessary for its installation and the knowledge that the higher SAS gains were not required for flight.

Interconnect-Ratio-Linkage Deadband

During checkout of the mechanical control system, a deadband was found in the linkage between the aileron and rudder surfaces, as shown in figure 21(a). The deadband was caused by the rudder cam mechanization. The deadband was mechanized on the M2-F2 simulator and found to be marginal for flight. The interconnect-ratio-linkage deadband, coupled with the aerodynamics, caused an initial roll reversal. As a result, each rudder surface was flared 5° to eliminate the deadband. Figure 21(b) illustrates the mechanization of the rudder cam with the rudders flared.
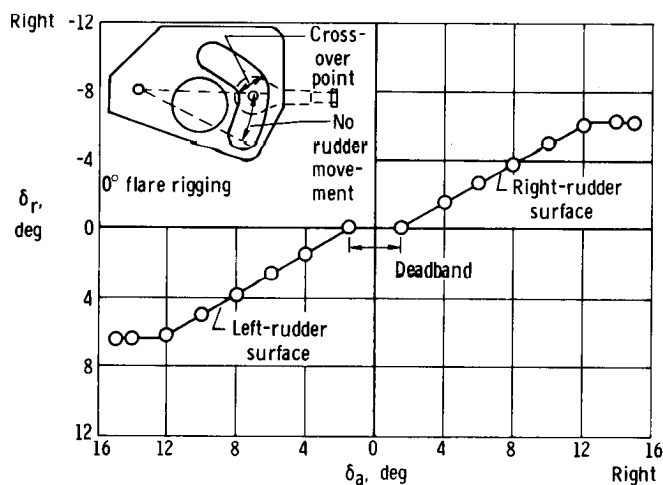
(a) Single surface movement; 0° flare.
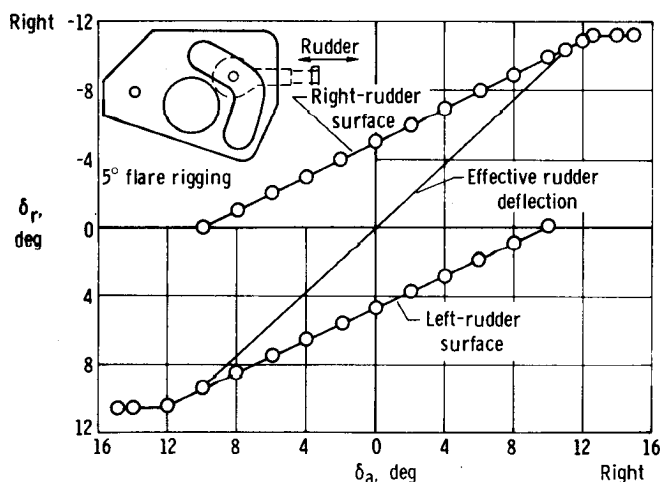
(b) Dual surface movement; 5° flare on each surface.

Figure 21.— *M2-F2 variation of rudder deflection with aileron deflection through the interconnect linkage.*

FLIGHT OPERATIONAL EXPERIENCES

Before the flight research program was started, the M2-F2 manual flight control system was extensively tested on the ground. The results of these ground tests revealed no instabilities in the basic flight control system, and none were encountered in flight. No significant deteriorations of the components of the control system were noted through usage.

Data obtained during M2-F2 flights were analyzed to determine the operational performance of the SAS. The study revealed that the system performed within design tolerances and operated at various gain settings with no apparent deterioration. No SAS failure occurred during flight.

Four pilots have flown the M2-F2 vehicle (ref. 10). They had no major difficulty in performing the required control tasks during normal flight. Roll control is not as positive as it is in some modern operational jet fighter aircraft because most of the M2-F2 roll control results from use of the rudders. For the rudder-to-aileron interconnect ratio (0.5) used in flight, the vehicle's roll control was predicted to be marginal in the low-angle-of-attack region (fig. 11). During a maneuver to obtain stability derivatives with an interconnect ratio of 0.5, the M2-F2 vehicle was sta-bilized at about -2° angle of attack and the roll- and yaw-damper gains were turned to zero. An aileron pulse was attempted; however, the vehicle rolled off and a pilot-induced oscillation (fig. 22) resulted even after the normal roll and yaw gains were set. During the oscillation, angles of attack as low as -5° were reached. Opposite aileron did not reduce the amplitude of the oscillation, but an increase in the angle of attack to about 8° resulted in roll-oscillation subsidence. Through the technique of neutralizing the ailerons and increasing the angle of attack, control of the vehicle was recovered.

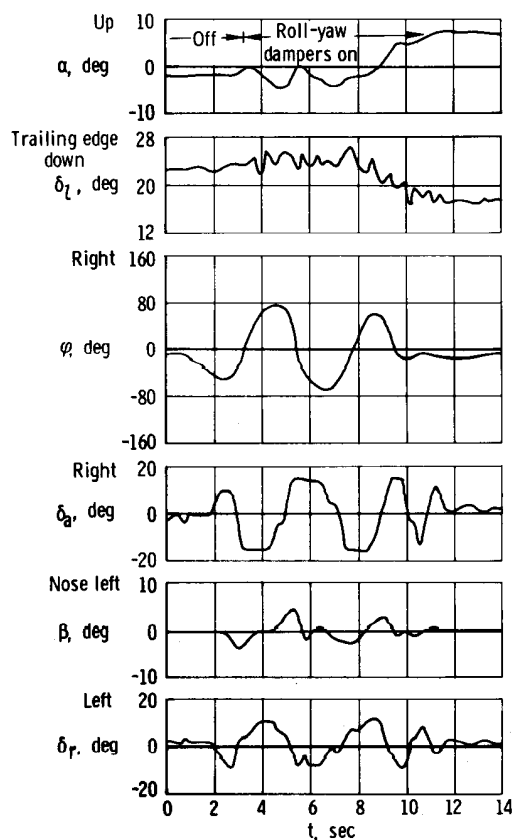
Figure 22.– *Time history of an M2-F2 lateral oscillation induced by the pilot and the stability augmentation system during flight. M = 0.61; h = 23,000 ft (7040 m) to 19,000 ft (5810 m); K_p = 0.4 deg/deg/sec; K_r = 0.6 deg/deg/sec; K_q = 0.6 deg/deg/sec; K_I = 0.5.*

The effect of changing the interconnect ratio is shown in figure 23, which illustrates the response of the vehicle at three different ratios to an aileron input. The angle of attack was 7°. Roll reversal was apparent for $K_I = 0.2$ (fig. 23(a)) as

aileron control was maintained and roll response was initially left as commanded but then reversed to right roll. At an interconnect ratio of 0.5 (fig. 23(b)), roll rate more nearly followed aileron control. Increased roll in the desired direction was evident (fig. 23(c)) at a higher interconnect ratio (0.8), thus indicating that roll induced by the rudder through the vehicle dihedral effect provided roll rates greater than with $K_I = 0.5$. Since it was planned that the interconnect ratio would remain fixed throughout each flight, a compromise value ($K_I = 0.5$) that resulted in sluggish roll control at high angles of attack and very sensitive roll control at low angles of attack was used in most of the flights.

(a) $K_I = 0.2$. (b) $K_I = 0.5$. (c) $K_I = 0.8$.
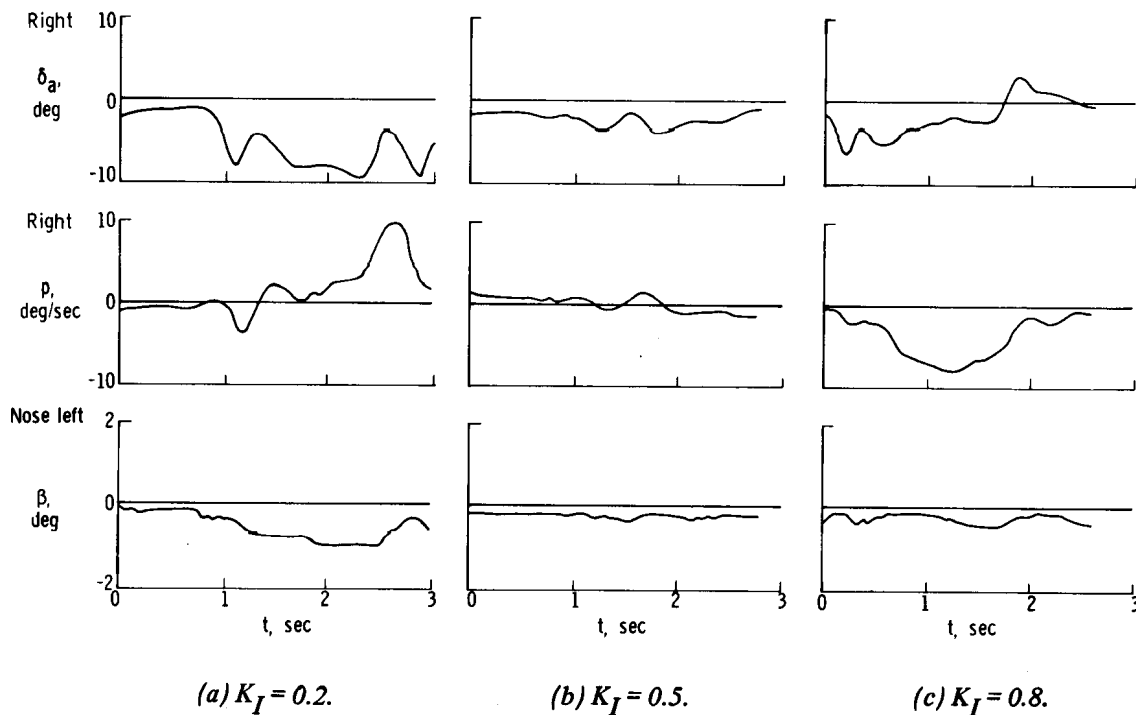
Figure 23.— Time histories of M2-F2 response to aileron inputs at three values of K_I. $\alpha = 7^o$; $K_p = 0.4$ deg/deg/sec; $K_q = 0.6$ deg/deg/sec; $K_r = 0.6$ deg/deg/sec.

With SAS on, vehicle motion was found to be well damped and was rated acceptable by the pilots, as shown in figures 24(a) to 24(c). With pitch SAS off, the pilots rated the vehicle adequately damped. With the roll-yaw dampers off, the vehicle was rated less acceptable than with the dampers on.

(a) Pitch axis.

	K_q, deg/deg/sec	K_p, deg/deg/sec	K_r, deg/deg/sec
———	0.6	0.4	0.6
- - -	0	.4	.6

(b) Roll axis.

	K_q, deg/deg/sec	K_p, deg/deg/sec	K_r, deg/deg/sec
———	0.6	0.4	0.6
- - -	.6	0	0

(c) Yaw axis.

	K_q, deg/deg/sec	K_p, deg/deg/sec	K_r deg/deg/sec
———	0.6	0.4	0.6
- - -	.6	0	0
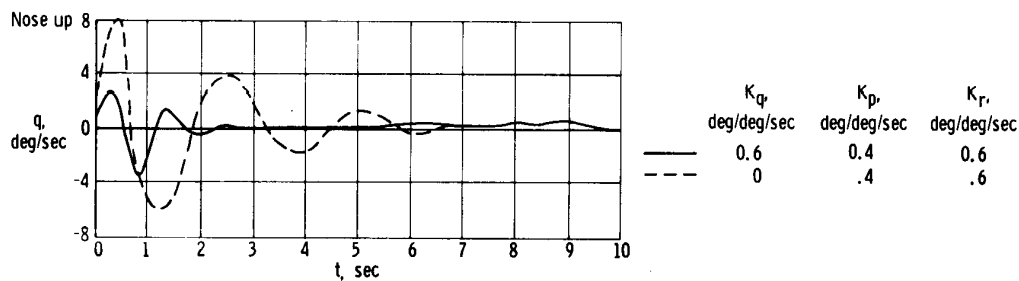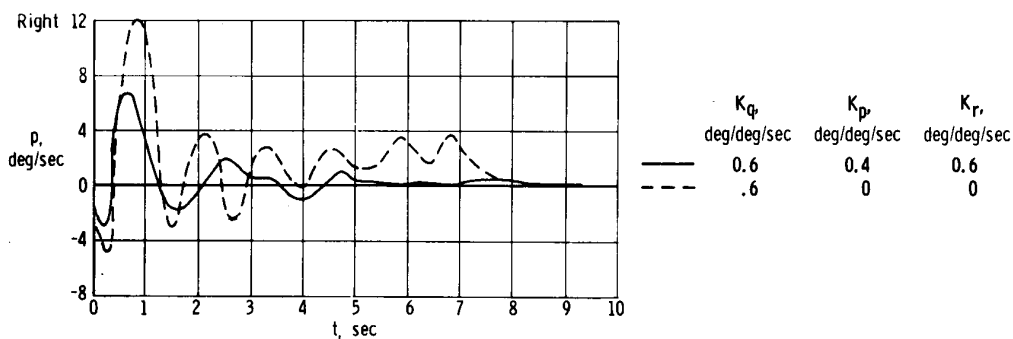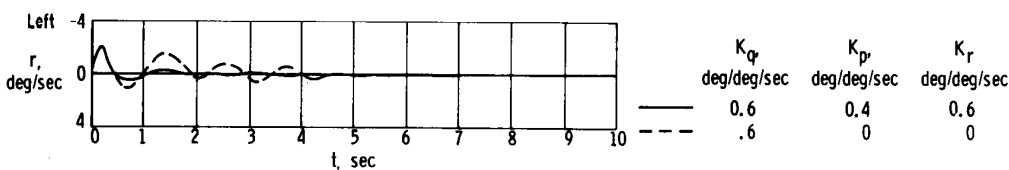
Figure 24.— Effects of SAS on M2-F2 damping characteristics. M = 0.56; $\alpha \approx 7^o$.

Limit cycles were experienced in flight during the approach to landing but had no adverse effect on the handling qualities of the vehicle (ref. 10). Limit-cycle data obtained during flight are compared with ground test data in figures 25 to 27. The ground-test results show good correlation with the flight results. No restriction of the SAS gain was required because of limit cycles. Maximum SAS gain used during flight was determined by structural resonance.

The pitch control was very positive, with more than enough g-capability to complete the flare.
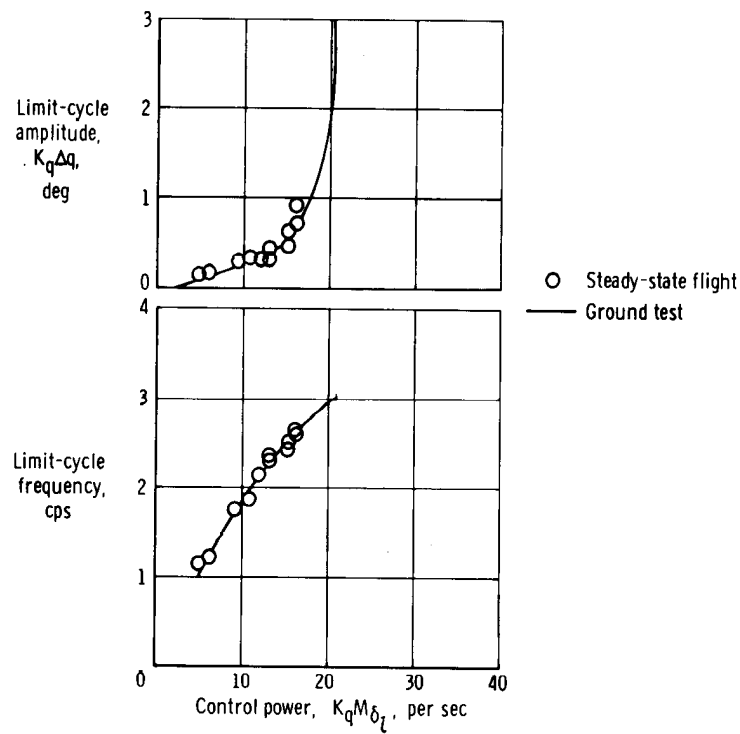
Figure 25. M2-F2 pitch SAS limit-cycle results.
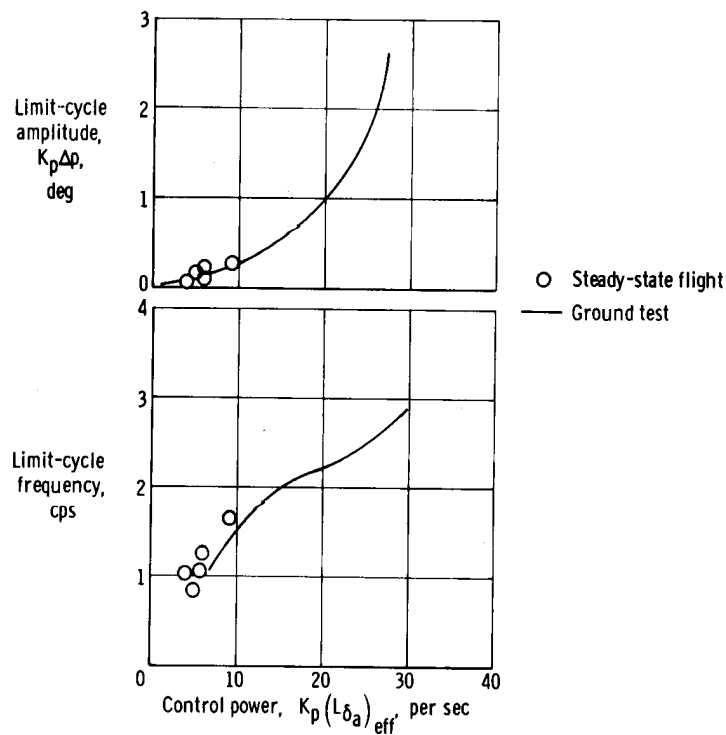
Figure 26. – M2-F2 roll SAS limit-cycle results.
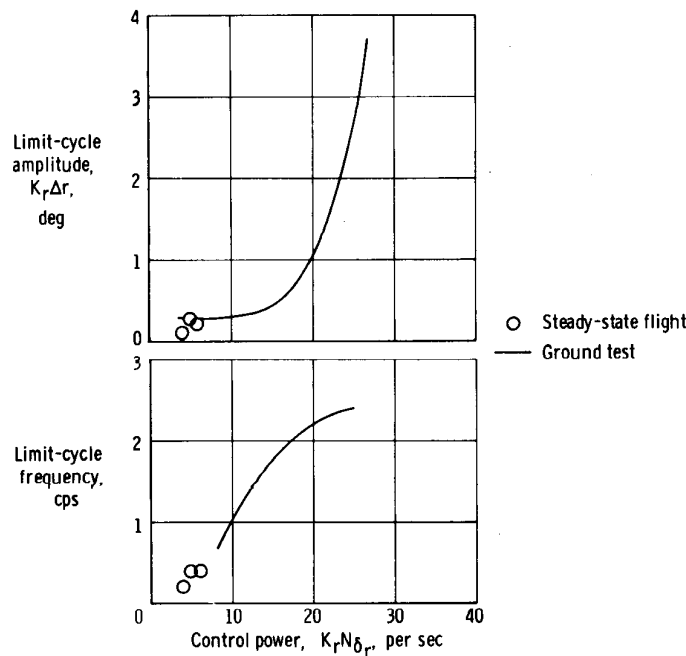
Figure 27.— M2-F2 yaw SAS limit-cycle results.
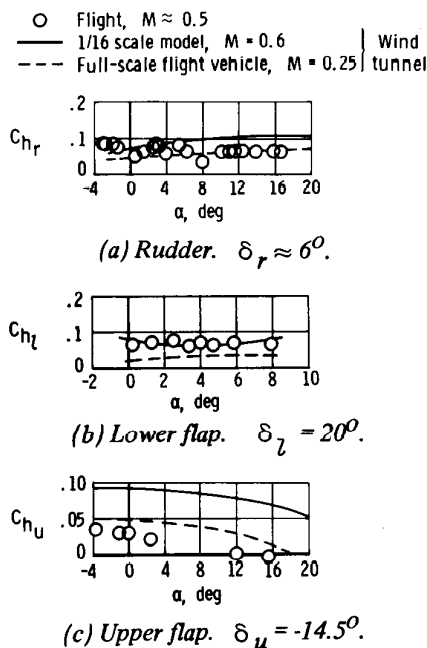
Figure 28.— Comparison of M2-F2 hinge-moment-coefficient data obtained in wind tunnels and flight.

Wind-tunnel and flight-determined hinge-moment-coefficient data (ref. 11) are compared in figure 28. In general, the results for the rudder (fig. 28(a)) and lower-flap (fig. 28(b)) surfaces showed good correlation, whereas the upper-flap (fig. 28(c)) flight data were lower in magnitude than the wind-tunnel data at the larger control deflections. Some of these discrepancies may have resulted from differences between the wind-tunnel-test conditions and the flight-test conditions. The wind-tunnel mounts that were used to support the M2-F2 model and vehicle during the wind-tunnel tests could have created flow patterns unlike those existing in flight. Also, the full-scale wind-tunnel tests were conducted at a steady-state Mach number of approximately 0.25, whereas the flight tests were conducted at varying Mach numbers from approximately 0.42 to 0.62.

27

CONCLUSIONS

Flight test and ground experience with the M2-F2 lifting body flight control systems led to the following conclusions:

1. The mechanical control system met the operational flight requirements for the test vehicle except for a deadband in the interconnect-ratio linkage between rudder and aileron. The deadband was effectively removed by flaring each rudder surface 5°.

2. A structural resonance encountered in early tests of the stability augmentation system was eliminated by filtering the electronic signals and stiffening the gyro mount.

3. The inability of the stability-augmentation-system monitor channel to track in the roll and yaw axes and the possibility of a hard-over condition being caused by the disengage circuitry led to a reduction of the stability-augmentation-system authority and deactivation of the roll and yaw monitor channels.

4. Electrical transients caused by normal cockpit switch operations caused stability-augmentation-system disengagements. This problem was eliminated by installing diodes across the switches to reduce the voltage transients and by installing a time-delay circuit in each magnetic switch circuit.

5. A limit cycle, or residual oscillation, was observed in all axes under flight conditions of high dynamic pressure and with relatively high stability-augmentation-system gains. This situation was alleviated by reducing system gain.

6. Longitudinal-control characteristics of the vehicle were acceptable.

7. The regions of pilot-induced oscillations predicted from ground simulation were encountered in flight. Lateral control of the vehicle was sluggish at high angles of attack and highly sensitive at low angles of attack.

8. Control-surface hinge moments experienced in flight correlated reasonably well with wind-tunnel predictions.

Flight Research Center,
National Aeronautics and Space Administration,
Edwards, Calif., February 14, 1969,
727-00-00-01-24.

REFERENCES

1. Stambler, Irwin: Manned Maneuverable Reentry. Space/Aeronautics, May 1964, pp. 44-52.

2. Horton, Victor W.; Layton, Garrison P., Jr.; and Thompson, Milton O.: Exploring New Manned Spacecraft Concepts. Astronaut. Aeron., vol. 2, no. 5, May 1964, pp. 42-47.

3. Smith, Harriet J.: Evaluation of the Lateral-Directional Stability and Control Characteristics of the Lightweight M2-F1 Lifting Body at Low Speeds. NASA TN D-3022, 1965.

4. Horton, Victor W.; Eldredge, Richard C.; and Klein, Richard E.: Flight-Determined Low-Speed Lift and Drag Characteristics of the Lightweight M2-F1 Lifting Body. NASA TN D-3021, 1965.

5. Pyle, Jon S.; and Swanson, Robert H.: Lift and Drag Characteristics of the M2-F2 Lifting Body During Subsonic Gliding Flight. NASA TM X-1431, 1967.

6. Holleman, Euclid C.: Stability and Control Characteristics of the M2-F2 Lifting Body Measured During 16 Glide Flights. NASA TM X-1593, 1968.

7. Durrett, John C.: Flight Planning and Conduct of the M2-F2 Glide Flight Program, Appendix III. FTC Tech. Rep. No. 67-13, U.S. Air Force, Sept. 1967.

8. Mechtly, E. A.: International System of Units - Physical Constants and Conversion Factors. NASA SP-7012, 1964.

9. Taylor, Lawrence W., Jr.; and Merrick, George B.: X-15 Airplane Stability Augmentation System. NASA TN D-1157, 1962.

10. Thompson, Milton O.; Peterson, Bruce A.; and Gentry, Jerauld R.: Lifting-Body Flight Test Program. SETP Technical Review, second 1966 issue, vol. 8, no. 2, Sept. 1966.

11. Jenkins, Jerald M.; Tang, Ming H.; and Pearson, George P. E.: Vertical-Tail Loads and Control-Surface Hinge-Moment Measurements on the M2-F2 Lifting Body During Initial Subsonic Flights Tests. NASA TM X-1712, 1968.

TABLE I. – PHYSICAL CHARACTERISTICS OF THE M2-F2 VEHICLE

Body –
    Planform area, feet^2 (meters^2):
        Actual 160 (14.9)
        Reference, S 139 (12.9)
    Longitudinal length, feet (meters):
        Actual 22.2 (6.76)
        Reference, c 20.0 (6.11)
    Span, without rudder flare, feet (meters):
        Actual 9.63 (2.94)
        Reference, b 9.54 (2.91)
    Aspect ratio, $\frac{b^2}{S}$, basic vehicle 0.655
    Body leading-edge sweep, degrees   77
Lower flap –
    Area, feet^2 (meters^2) 15.23 (1.41)
    Span, feet (meters) 5.42 (1.65)
    Chord, feet (meters) 2.81 (0.86)
    Deflection, degrees:
        Pilot's control authority, down   . . . .   5 to 30
        Pitch stability-augmentation-system authority . . . .   ±5
    Design hinge moment, inch-pounds (newton-meters) 67,000 (7560)
Upper flaps, two –
    Area, each, feet^2 (meters^2) 9.57 (0.89)
    Span, each, feet (meters) 4.28 (1.31)
    Chord, feet (meters) 2.23 (0.68)
    Deflection, degrees:
        Pitch trim (symmetric travel), up   . . . .   0 to 35
        Pilot's aileron authority (differential upper flap travel)   . . . .   ±10
        Roll stability-augmentation-system authority (differential
            upper-flap travel) . . . .   ±5
    Design hinge moment, each, inch-pounds (newton-meters) 30,000 (3380)
Vertical stabilizers, two –
    Area, each, feet^2 (meters^2) 16.10 (1.50)
    Height, trailing edge, feet (meters) 3.79 (1.16)
    Chord, feet (meters):
        Root 7.36 (2.24)
        Tip 2.58 (0.79)
    Leading-edge sweep, degrees 62.3
Rudders, two –
    Area, each, feet^2 (meters^2) 5.27 (0.49)
    Span, each, feet (meters) 4.20 (1.28)
    Chord, feet (meters) 1.25 (0.38)
    Deflection, each (outward), degrees:
        Pilot's effective control authority   11
        Yaw stability-augmentation-system authority 4.2
    Design hinge moment, each, inch-pounds (newton-meters) 23,000 (2595)
Weight, including pilot, pounds (kilograms) 6000 (2722)
Center of gravity:
    Percentage of actual length   49
    Percentage of reference length   54
Planform-area loading, $\frac{W}{S}$, pounds/foot^2 (kilograms/meter^2) 43.2 (196)

Moments of inertia –
    I_X, slug-foot^2 (kilogram-meter^2) 956.3 (1296)
    I_Y, slug-foot^2 (kilogram-meter^2) 5583 (7570)
    I_Z, slug-foot^2 (kilogram-meter^2) 6005 (8142)
    I_{XZ}, slug-foot^2 (kilogram-meter^2) . . . .   -417 (-565)